Annual Methodological Archive Research Review
http://amresearchreview.com/index.php/Journal/about
Volume 3, Issue 10 (2025)

Online ISSN 3007-3197
Print ISSN 3007-3189

http://amresearchreview.com/index.php/Journal/about

Investigation of Structural and Optical Properties of Copper Oxide Nanoparticles Applicable in Flexible and Transparent Windows

Azaz Javed
Department of Basic Sciences, Superior University Lahore
Email: SU92-MPPHW-F23-005@superior.edu.pk

Sumyya Dhiloon
Department of Basic Sciences, Superior University Lahore
Email: Su92-mpphw-f23-007@superior.edu.pk

Syed Muzaffer Ali Shah
Department of Basic Sciences, Superior University Lahore
Email: Su92-mpphw-f23-008@superior.edu.pk

ABSTRACT

In this work, glucose is used as the reducing agent and $CuCl_2$ as the precursor to create Cu, CuO and Cu_2O NPs by a chemical reduction method. By using X-ray diffraction (XRD), energy dispersive X-ray (EDX) and scanning electron microscopy (SEM), the Cu, CuO and Cu_2O NPs structure and morphology are studied. The generation of Cu, CuO and Cu_2O NPs is confirmed by the UV-Visible absorption spectra, which exhibit peaks at 559, 558 and 557 nm, respectively. The three samples are prepared at different growth temperatures i.e. 60^0, 70^0 and 80^0, named as Cu-T_1, Cu-T_2 and Cu-T_3, respectively. Using Tauc plots and absorption data, the band gaps of the Cu-T_1, Cu-T_2 and Cu-T_3 NPs are found to be 2.04 eV, 2.15 eV and 2.21 eV, respectively. The XRD patterns demonstrates the crystalline and monoclinic nature of the Cu, CuO and Cu_2O NPs. The crystallinity of Cu, CuO and Cu_2O NPs is likewise shown to rise with an increase in annealing temperature and the diffraction peaks are made sharper. The structural analyses exhibit base-centered spherical nanocrystals with crystallite sizes of 12 nm, 23 nm and 18 nm for the said samples. The SEM images reveal the corresponding non-agglomerated particle diameters of about 310 nm, 200 nm and 100 nm, respectively. To obtain the optical responses from Cu_2O NPs, hydroxyl ethyl cellulose (HEC) as an adhesive agent mixed with the sample "Cu-T_3 NPs" is used as an ink and spread on a flexible substrate (Polyethylene-terephthalate/PET) with different dispersion volumes (0 mL, 0.04 mL, 0.08 mL, 0.12 mL, 0.16 mL and 0.2 mL). As prepared flexible substrate-based sample are tested for their transmittance measurements. The maximum transmittance obtained is 82.37% for 0.04 mL dispersion and the minimum value is 53.23% for 0.2 mL dispersion ink, suggesting the Cu_2O NPs desirable candidates for low cost flexible and transparent windows applicable in solar panels and other technologies.

Annual Methodological Archive Research Review
http://amresearchreview.com/index.php/Journal/about
Volume 3, Issue 10 (2025)

Online ISSN 3007-3197
Print ISSN 3007-3189

http://amresearchreview.com/index.php/Journal/about

Introduction

In recent years, the nanoscale realm has unveiled unprecedented opportunities to engineer materials with tailor-made properties that surpass those of their bulk counterparts. Among these, copper nanoparticles stand out due to their exceptional combination of electrical, catalytic, and antimicrobial characteristics, which are intricately linked to their nanoscale dimensions and high surface reactivity[1-3]. As copper transitions from a conventional bulk metal to a nanosized form, it acquires enhanced physicochemical behaviors that have unlocked new frontiers in applications ranging from energy and electronics to environmental remediation and biomedicine[3, 4]. This unique transformation at the nanoscale motivates ongoing research into efficient, sustainable synthesis methods and innovative applications of copper nanoparticles[5]. Copper nanoparticles are especially attractive because of their high electrical conductivity, catalytic efficiency, and intrinsic antimicrobial properties[6-9]. These features make them valuable in developing super-strong composite materials, sensors, catalysts, and antibacterial agents. The growing demand for copper nanoparticles in various industrial and biomedical fields has driven the search for effective synthesis methods that are both cost-efficient and environmentally sustainable[10-12].

The synthesis of nanoparticles broadly follows two approaches: Top-Down and Bottom-Up methods. The Top-Down approach involves breaking down bulk materials into nanoscale particles through physical or mechanical processes[13-15]. In contrast, the Bottom-Up approach builds nanoparticles atom-by-atom or molecule-by-molecule, typically via chemical or biological synthesis. The Bottom-Up method offers greater control over particle size, shape, and composition, allowing for tailoring of properties specific to desired applications[16-18]. Conventional physical and chemical synthesis techniques, although effective, often involve hazardous chemicals, high energy consumption, and may generate toxic byproducts, raising concerns about environmental and human health impacts. In response, green synthesis strategies have gained prominence. These methods employ biological materials such as plant extracts, microorganisms, or natural biomolecules as reducing and stabilizing agents, providing an eco-friendly, cost-effective, and sustainable alternative to conventional methods. Green-synthesized copper nanoparticles tend to exhibit improved biocompatibility and reduced ecotoxicity[19-21].

Copper nanoparticles produced via green synthesis have found growing use in agriculture as nano-fertilizers and nano-insecticides that enhance crop yield and protect against pathogens. Furthermore, their role in environmental remediation—particularly in wastewater treatment and heavy metal removal—highlights their importance in addressing pressing ecological challenges. The excellent electrical conductivity of copper nanoparticles also underpins their application in advanced electronics and superconductors. Despite the advances in nanoparticle synthesis, many traditional methods suffer from limitations such as poor control over particle morphology, low production yields, high operational costs, and significant energy demands[22, 23]. Therefore, developing safe, non-toxic, and scalable synthesis routes remains a critical objective in nanoparticle research. In conclusion, copper nanoparticles represent a versatile class of nanomaterials whose unique physicochemical and biological properties have opened new avenues across scientific

Annual Methodological Archive Research Review
http://amresearchreview.com/index.php/Journal/about
Volume 3, Issue 10 (2025)

Online ISSN 3007-3197
Print ISSN 3007-3189

http://amresearchreview.com/index.php/Journal/about

and industrial domains. Continued efforts in green synthesis and application development will further accelerate their integration into next-generation technologies[24, 25].

This research focuses on the synthesis of copper oxide nanoparticles via green synthesis methods and their comprehensive characterization to explore potential applications. The study aims to investigate the optical, structural, and morphological properties of the synthesized nanoparticles using ultraviolet-visible (UV-Vis) spectroscopy, Fourier transform infrared (FTIR) spectroscopy, powder X-ray diffraction (PXRD), and scanning electron microscopy (SEM). Special attention will be given to understanding the band gap energy, functional groups, crystallinity, and surface morphology of the nanoparticles. The outcomes of this research will contribute to optimizing the synthesis process and evaluating the suitability of copper oxide nanoparticles for applications in antibacterial activity, catalysis, and environmental remediation.

Materials and Methods

Preparation of Copper Oxide Nanoparticles

A modified synthesis method was followed [72]. The usual synthesis technique was as follows: A copper precursor solution was created by combining $CuCl_2$ (767.16 mg), TEA (971.1 uL), KOH (198.03 g) and DIW (300 mL). It had a constant molar ratio of $CuCl_2$ to TEA at 1:3 and the KOH concentration was set at 3.529 M. In order to make a 30 wt% reducing solution, glucose was dissolved in DIW. After that, the copper precursor solution was poured into a beaker and heated to 80 ℃. The reaction system was then pipetted with the reducing solution and the stir bar was removed after around 5 min of vigorous stirring.

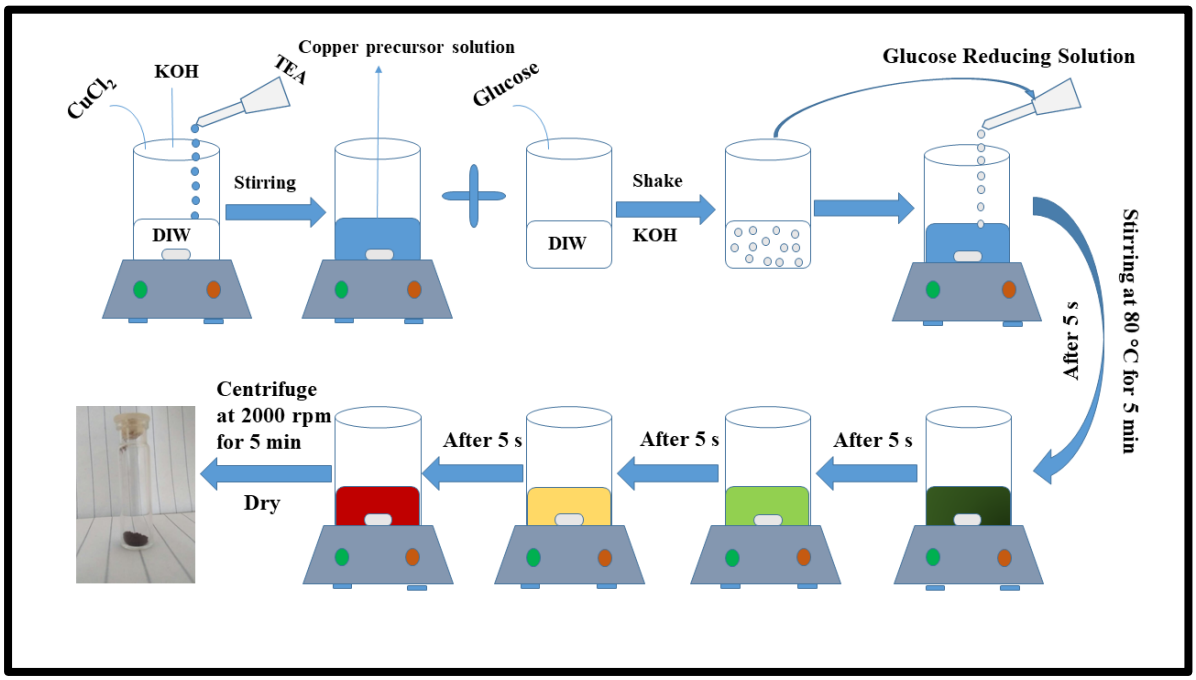


Figure Error! No text of specified style in document..**1:** Synthesis mechanism of Cu,

Annual Methodological Archive Research Review
http://amresearchreview.com/index.php/Journal/about
Volume 3, Issue 10 (2025)

Online ISSN 3007-3197
Print ISSN 3007-3189
http://amresearchreview.com/index.php/Journal/about

CuO and Cu_2O NPs.

Every 5 seconds, the solution went from sea green to light green to yellowish and then quickly to dark red. The reaction was done when a dark red floc developed and floated on top of the aqueous solution. The floc was recovered by centrifugation at 2000 rpm for 5 min and then re-dispersed in ethanol. The centrifugation and re-dispersion procedure was carried out three times to remove the reaction residues from the surface of the CuNP. Washed three times with absolute ethanol After that, we left the ingredients in the petri dish for drying purposes at room temperature. Finally, grind the sample as fine as possible. Also, we have obtained nanoparticles by chemical reduction method.

Preparation of Copper, Cupric Oxide and Cuprous Oxide Based Ink

In order to prepare the Cu, CuO and Cu_2O based ink, hydroxyethyl cellulose (HEC) was used as a specialty glue. Initially, 25 mL of DIW was mixed with 0.25 g of HEC using gentle stirring. After that, 8.7 mL of ethanol in a beaker was used to dissolve 28.7 mg of Cu NPs while maintaining moderate mixing. 4 mL of the HEC arrangement were added dropwise to the solution after a little while. Another 4 mL of HEC solution was added after 15 min. Finally, the mixture was stirred for 2 to 3 hours to completely melt the Cu, CuO and Cu_2O in HEC and distribute them evenly throughout the solution.

Preparation of Copper, Cupric Oxide and Cuprous Oxide Nanoparticles Coated Flexible PET Films

Using a mechanically demanding approach and the Meyer rod, flexible PET films were created. First, 4x4 cm squares of a clear PET film with remarkable flexibility were placed on a perfectly level surface. The first piece of PET film was then covered with 0 mL, 0.04 mL of the composite ink solution using a pipette, which was followed by mechanical folding and in any case spreading the ink using a Meyer rod. The films were then evenly inked and sintered for around three minutes at 130 ^{0}C in a preheated oven. Five PET film pieces were located using various quantities of ink (0.04 mL, 0.08 mL, 0.12 mL, 0.16 mL and 0.2 mL). The films could finally be dried under a vacuum.

Results and Discussion

UV-Visible Absorption Spectroscopic Studies

The spectroscopic analysis of Cu, CuO and Cu_2O NPs was done by using the UV-Vis absorption spectroscopy instrument. **Figure 4.1** gives the results of UV-Vis absorption spectra for the samples i.e. Cu-T_1, Cu-T_2 and Cu-T_3. All three samples were prepared under different temperatures in the reaction. It is observed that the sample Cu-T_1 shows the peak maxima at a wavelength of 559.1 nm and sample Cu-T_2 shows the peak maxima at 558.2 nm. Similarly, sample Cu-T_3 shows the peak maxima at 557.5 nm.

Annual Methodological Archive Research Review
http://amresearchreview.com/index.php/Journal/about
Volume 3, Issue 10 (2025)

Online ISSN 3007-3197
Print ISSN 3007-3189

http://amresearchreview.com/index.php/Journal/about

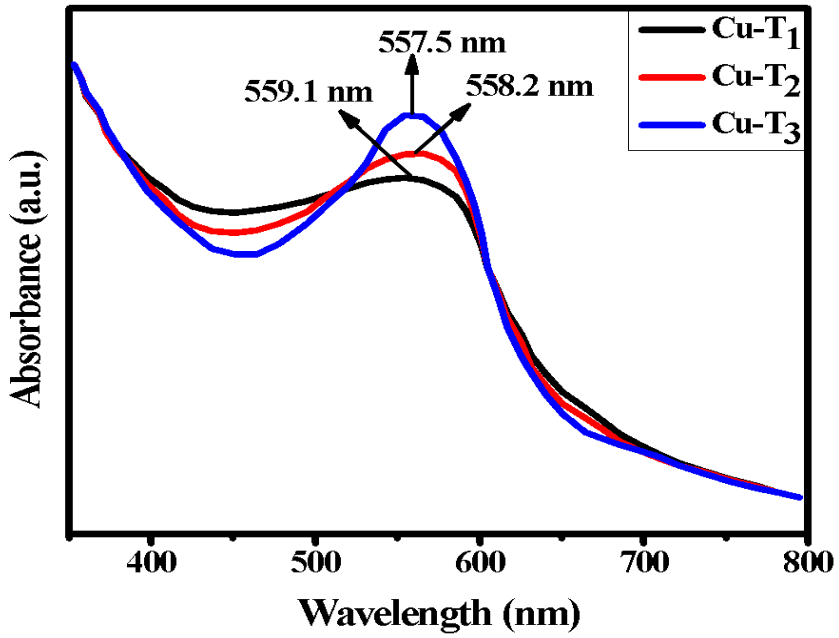


Figure Error! No text of specified style in document..**2:** UV-Vis spectra of Cu-T_1, Cu-T_2 and Cu-T_3 samples showing the three different peaks at 559.1 nm, 558.2 nm and 557.5 nm, respectively.

Shifting in absorbance peaks from the red to blue wavelength region indicates the decrease in particle size usually [26]. Hence, the heat treatment time affected the size of nanostructures. Therefore, the heat-treated time affected the UV-Vis absorption spectra of Cu-T_1, Cu-T_2 and Cu-T_3 nanostructures in three ways; increase in the peak maxima, shifting of the peak and the peak contracting [27].

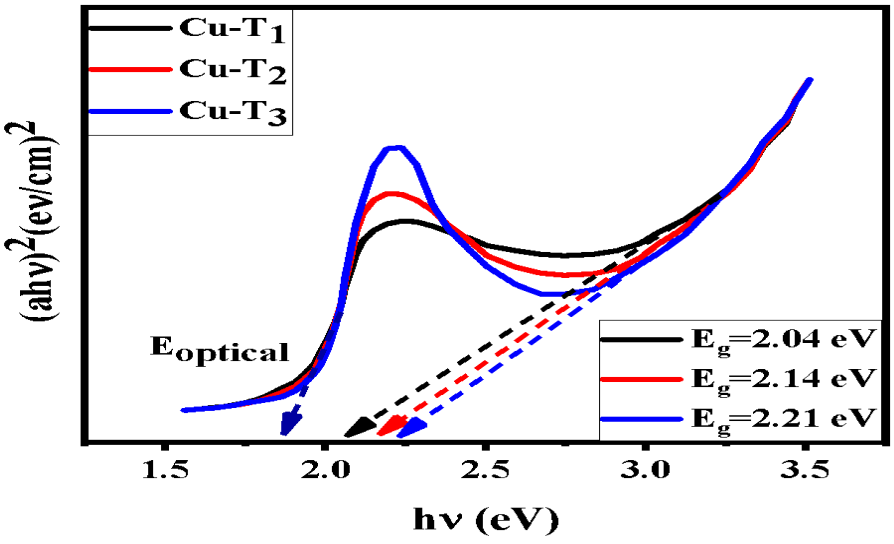


Figure Error! No text of specified style in document..**3:** The band gap measurements

Annual Methodological Archive Research Review
http://amresearchreview.com/index.php/Journal/about
Volume 3, Issue 10 (2025)

Online ISSN 3007-3197
Print ISSN 3007-3189

http://amresearchreview.com/index.php/Journal/about

of Cu-T_1, Cu-T_2 and Cu-T_3 nanoparticles grown at different temperatures.
The Cu-T_1, Cu-T_2 and Cu-T_3 nanoparticles have shown band gaps of 2.04 eV, 2.14 eV and 2.21 eV, respectively, as calculated from the absorption data using Tauc plots. The increase in band gap was due to the quantum confinement of carriers within the small dimension of nanostructures [28]. It was found that the Tauc plots of all samples of nanoparticles contained a single peak of all the samples corresponding to the optical band gap ~ 1.8 eV. According to band theory, the first transition at a larger wavelength corresponds to an optical band gap due to the optical absorption and the formation of bonded electron-hole pair or exciton "Frankel exciton". Whereas, the second transition at a lower wavelength is the energy gap between the valence and the conduction band [29].

X-Ray Diffraction Analysis

According to the XRD pattern, the produced nanoparticles are a combination of metallic Cu, CuO and Cu_2O. Miller indices of (111) and (200) for the copper lattice planes in the XRD patterns for the pure crystalline metallic phase Cu NPs suggest a small degree of variation for the monoclinic structure, which is observed at 43.04^0 and 50.3^0. The particle size distribution of Cu NPs is responsible for the modest shifting (concerning JCPDS.No.01-085-1326). The loss of crystallinity is shown by a decrease in the diffraction peaks of Cu. Cu nanoparticles are oxidized with oxygen present in the air and converted into CuO and Cu_2O.

Annual Methodological Archive Research Review
http://amresearchreview.com/index.php/Journal/about
Volume 3, Issue 10 (2025)

Online ISSN 3007-3197
Print ISSN 3007-3189

http://amresearchreview.com/index.php/Journal/about

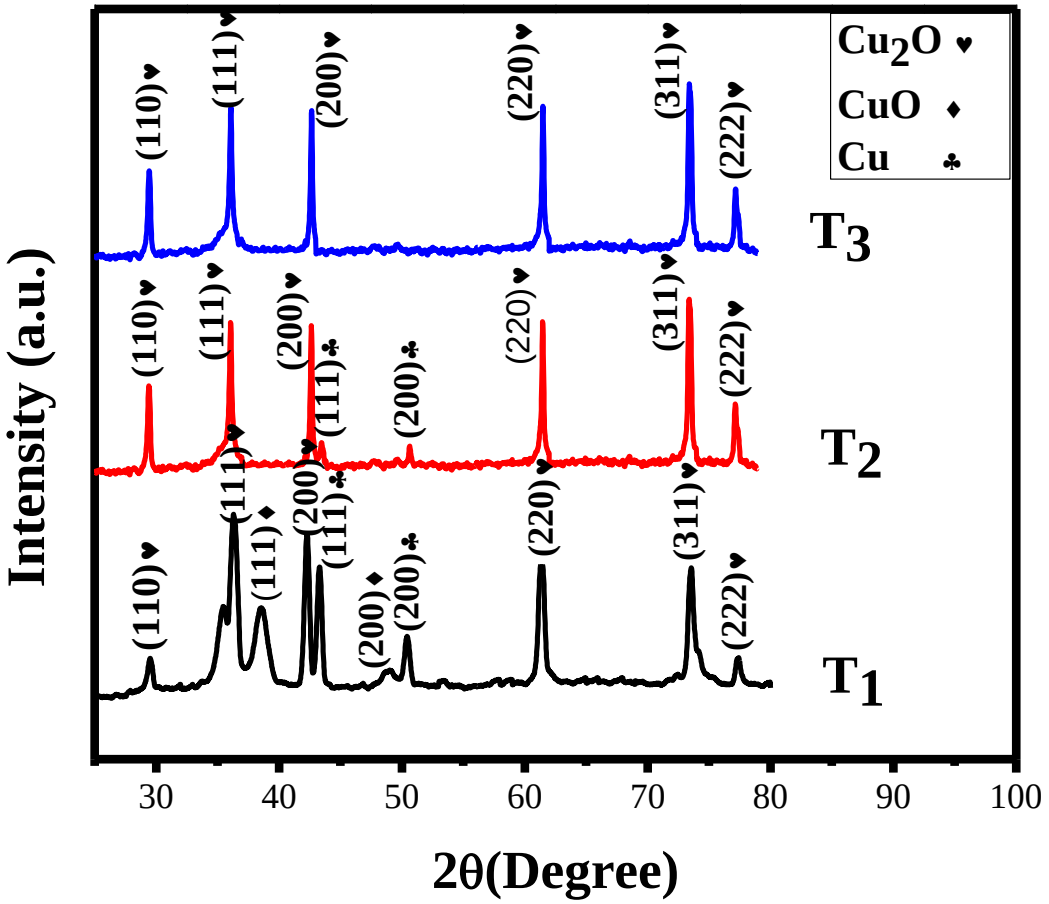


Figure Error! No text of specified style in document.**.4:** XRD pattern of Cu, CuO and Cu_2O nanoparticles.

When the created Cu NPs were placed in the air, CuO and Cu_2O developed on their surface, as shown in **Figure 4.3**. As CuO with indices of 38.5^0 and 48.2^0 which correspond to crystal planes (111) and (220) and Cu_2O with indices of 29.3^0, 36.1^0,42.2^0,61.3^0,73.5^0 and 77.2^0 which correspond to crystal planes (110), (111) and (200), (220), (311) and (222) Cu_2O chemical composition was expected, as the capping molecules occupied a major portion of the surface and oxidation would take place when the LSPR band intensity of crystalline Cu_2O NPs gradually increased. The obtained results are comparable to past findings for both copper and its oxides [30]. It was found that the matching peak's strength and broadness varied. The strength of all diffraction peaks increases as temperature rises, while their full width at half maximum (FWHM) decreases. Thus, the average Cu_2O crystal size may be approximated as 12.58 nm based on the FWHM of the diffraction peaks of the (111) plane of Cu_2O, demonstrating that the crystallinity of Cu_2O increased with increasing temperature. Heat-induced crystallite development of Cu_2O leads to increased crystallinity because better ordering in the structure of Cu_2O makes the X-ray peak sharper and narrower. In all annealing temperatures, the signal at 36.1° was consistently prominent, showing that these Cu_2O samples contain strongly aligned (111) planes. Since at decreased temperature, the reaction thermodynamics was weak and the rate of thermodynamics slow but the reaction kinetics were higher which

Annual Methodological Archive Research Review
http://amresearchreview.com/index.php/Journal/about
Volume 3, Issue 10 (2025)

Online ISSN 3007-3197
Print ISSN 3007-3189
http://amresearchreview.com/index.php/Journal/about

resulted in the oxidation of Cu nanoparticles finally forming CuO and Cu_2O nanoparticles. Further increase of temperature reaction thermodynamics also adds so we get a higher degree of oxidation of Cu nanoparticles with oxygen present in the environment [31].

When we raise 80^0 we get the product consisting of only Cu_2O nanoparticles. After the heat treatment, no more impurity peaks were discovered and there was no significant change in the positions of the peaks in the XRD spectra, suggesting that Cu_2O was achieved. The nanoparticles are bigger at lower temperatures and as the temperature rises throughout the process, the size increases. The lattice structure of CuO-NPs annealed at 80˚C is almost base-centered monoclinic. With increasing annealing temperature, the average crystallite size of CuO-NPs was increased. With increasing annealing temperature, the atoms in CuO-NPs diffuse across the boundaries of the particles, fusing the particles and creating one larger particle. Therefore, the crystallite size of the samples increases with increasing the annealing temperature. Higher annealing temperature led to a larger crystallite size of CuO-NPs because higher annealing temperature means higher energy given which results in more oxidation [13, 32].

Calculation of the Average Lattice Size of Copper Oxide Nanoparticles

The prepared samples lattice size (D) may be determined using the Debye-Scherrer equation, which has the following numerical form

$$D = 0.9 \times \frac{\lambda}{\beta COS\theta}$$

Where,

λ = is the X-ray wavelength used in the experiment.
β = maximum intensity at half width
θ = Braggs angle

According to the Scherrer formula, D has values of 12.58 nm, 23.92 nm and 18.08 nm for Cu, CuO and Cu_2O nanoparticles.

Table Error! No text of specified style in document.**.1:** Lattice parameters of Cu-T_1, Cu-T_2 and Cu-T_3 nanoparticles.

Annual Methodological Archive Research Review
http://amresearchreview.com/index.php/Journal/about
Volume 3, Issue 10 (2025)

Online ISSN 3007-3197
Print ISSN 3007-3189

http://amresearchreview.com/index.php/Journal/about

Sample ID	(hkl)	2Θ	Beta(β)	a(Å)	c(Å)	c/a	Size of lattice D(nm)	Strain	Dislocation density	Lattice spacing (d) Å
Cu-T1	110	29.5085	0.49821	4.04399	2.87324	0.7105	16.4829	0.12045	0.0036807	0.30235
	111	36.1488	1.41428				5.90647	0.33612	0.0286645	0.24819
	111	38.5581	1.14648				7.3381	0.27055	0.0185709	0.23321
	200	42.2817	0.46706				18.2294	0.10891	0.0030092	0.2135
	111	43.2959	0.44976				18.9964	0.10451	0.0027711	0.20873
	220	48.2959	84.011				0.10359	19.1648	93.187701	0.18822
	200	50.4274	0.5043				17.4052	0.11406	0.003301	0.18075
	220	61.3707	0.5692				16.223	0.12238	0.0037996	0.15088
	311	73.5542	0.59636				16.625	0.11942	0.0036181	0.12861
	222	77.8441	29.1713				0.3499	5.67383	8.1677225	0.12256
Cu-T2	110	29.4134	0.29606	3.97562	2.78953	0.70166	27.7315	0.07159	0.0013003	0.3033
	111	36.0579	0.42393				19.6996	0.10078	0.0025768	0.24879
	200	42.6292	0.24825				34.3374	0.05782	0.0008481	0.21184
	111	43.4656	0.3566				23.9732	0.08281	0.00174	0.20795
	200	59.3612	572.032				0.01598	124.245	3916.5907	0.1555
	220	61.4596	0.27622				33.4458	0.05936	0.000894	0.15069
	311	73.4216	0.35936				27.5654	0.07202	0.001316	0.12881
	222	77.1909	0.4123				24.6436	0.08056	0.0016466	0.12343
Cu-T3	110	29.5128	0.30162	4.23143	4.16448	0.98418	27.2265	0.07292	0.001349	0.3023
	111	36.1565	0.48024				17.3946	0.11413	0.003305	0.24813
	200	42.7282	0.29551				28.8557	0.0688	0.001201	0.21137
	220	61.5559	0.36736				25.1606	0.0789	0.0015796	0.15048
	311	73.5211	0.40056				24.7462	0.08023	0.001633	0.12866
	222	77.2929	0.47686				21.3224	0.09311	0.0021995	0.1233

Scanning Electron Microscopic Analysis

To obtain accurate visual surface images of samples, is an essential approach. While acquired topography describes the surface characteristics of the target material, such as its texture, smoothness and roughness, morphology in SEM photographs specifies the shape and size of the object.

In **Figure 4.4** below, the SEM images of the Cu, CuO and Cu_2O NPs are displayed. Cu, CuO and Cu_2O NPs are distributed densely and randomly as shown in the image to generate large-scale rod-like and sphere-like nanostructures. The nanoparticles range in size from a few nanometers to a few micrometers and their length and width are random. The manufactured product is made up of spherical nanoparticles with a limited size distribution, according to the SEM image [33, 34].

Figure 4.5 shows that the shape of Cu_2O did not change when annealed at 60 °C. However, when the annealing temperature increased, Cu_2O NPs with rod-like and sphere-like nanostructures vanished, and the original Cu_2O NPs expanded into huge manners with diameters ranging from hundreds of nanometers to several micrometers. When Cu_2O NPs were annealed at 70 °C, a phase coexistence of Cu_2O and Cu was detected due to the appearance of two new peaks $2\theta = 43.2°$, 50.4° corresponding to

Annual Methodological Archive Research Review
http://amresearchreview.com/index.php/Journal/about
Volume 3, Issue 10 (2025)

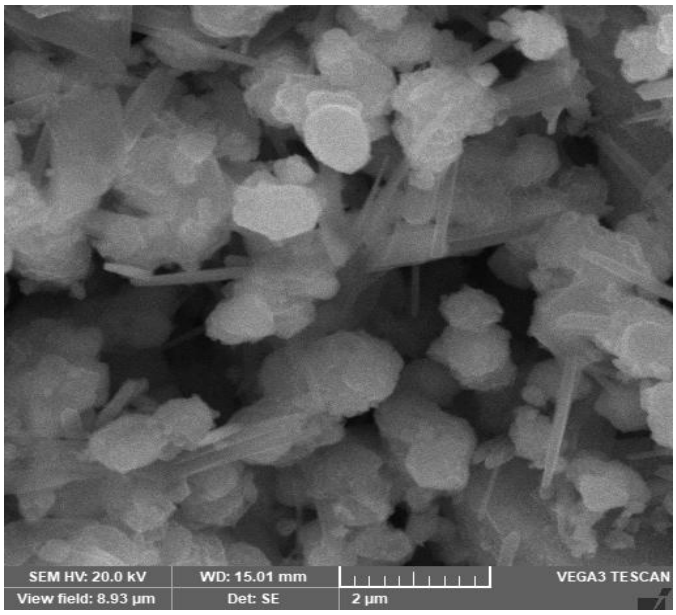
Online ISSN 3007-3197
Print ISSN 3007-3189

http://amresearchreview.com/index.php/Journal/about

the planes (111), (200) of copper (JCPDS card No.04-0836) and the other at 77.25° corresponding to the plane (222) of Cu_2O [35].

$2Cu_2O \rightarrow Cu + O_2$

Figure 4.6 shows Cu, CuO and Cu_2O NPs are possible due to their tiny particle size, large surface area and strongly (111) plane-oriented crystal composition. Cu_2O NPs, on the other hand, are more susceptible to photo corrosion than Cu_2O micro particles. The temperature at 80 °C produced a SEM picture of Cu_2O NPs. The SEM image of Cu_2O NPs revealed that the particles are well-dispersed spherical with a nearly well-defined and homogeneous crystalline structure. There was also a strong tendency towards agglomerations [36].



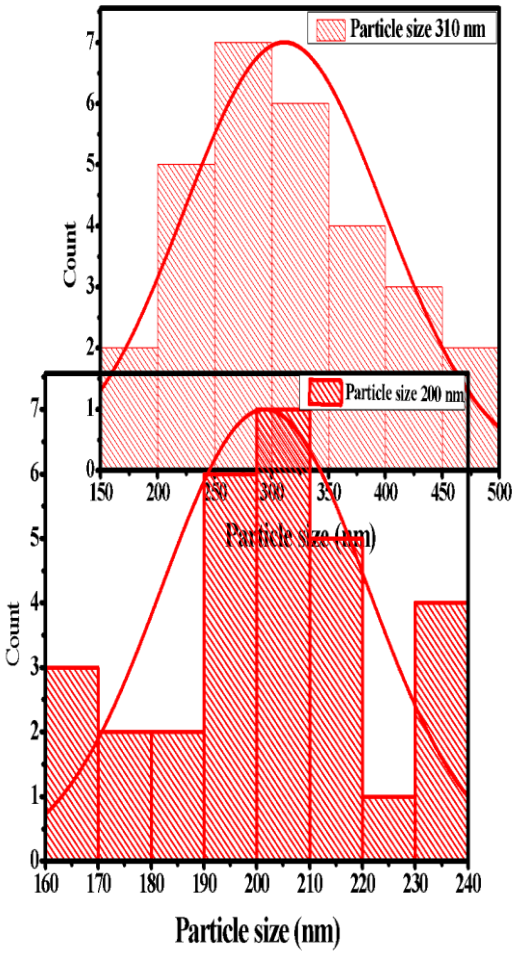
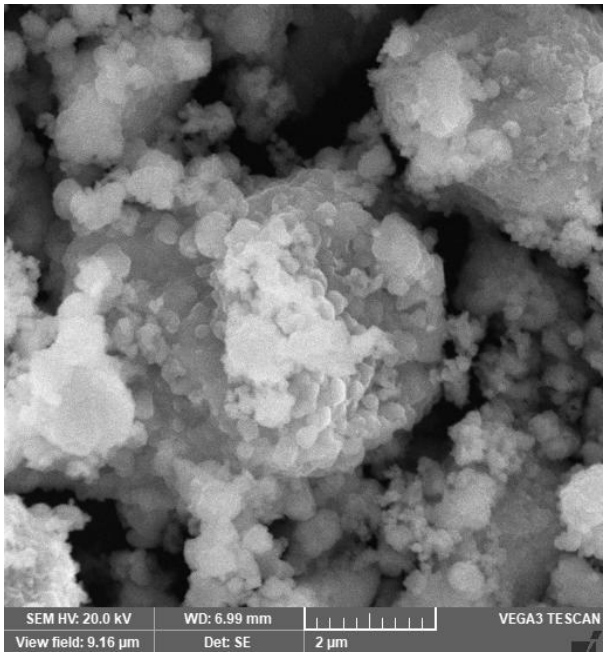


Figure Error! No text of specified style in document..**5:** SEM images of Cu, CuO and Cu_2O rod-like and sphere–like nanoparticles.

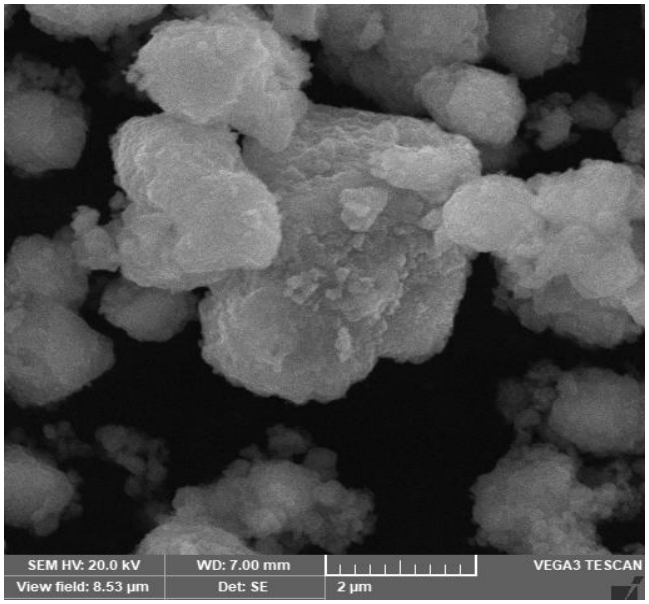


Annual Methodological Archive Research Review
http://amresearchreview.com/index.php/Journal/about
Volume 3, Issue 10 (2025)

Online ISSN 3007-3197
Print ISSN 3007-3189

http://amresearchreview.com/index.php/Journal/about

Figure Error! No text of specified style in document.**.6:** SEM images of Cu, CuO and Cu_2O NPs.



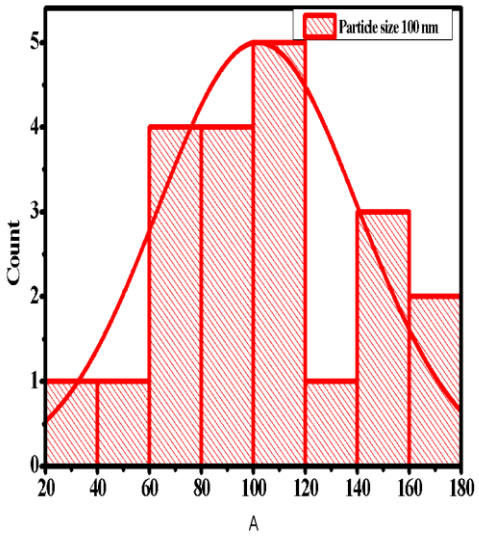


Figure Error! No text of specified style in document.**.7:** SEM images of Cu, CuO and Cu_2O NPs are tiny particle sizes.

Energy Dispersive X-Ray Analysis (EDAX)

The elemental mapping of the components found in the Cu, CuO and Cu_2O nanoparticle sample that was synthesized is shown in **Figures 4.7**. Energy dispersion X-ray spectra reveal that the nearly spherical Cu_2O nanostructure particles in **Figure 4.7** contain Cu, O and K with weights of 76.12, 20.76, and 3.12, respectively. According to the appropriate elemental mapping in

Figure 4.7 (i), (ii), and (iii) for Cu nanostructures, Cu and O are organized well and in relatively tiny amounts, respectively. The absence of additional elements from the EDAX spectrum shows that the generated Cu, CuO and Cu_2O NPs are compatible with the XRD findings [36].

Annual Methodological Archive Research Review
http://amresearchreview.com/index.php/Journal/about
Volume 3, Issue 10 (2025)

Online ISSN 3007-3197
Print ISSN 3007-3189

http://amresearchreview.com/index.php/Journal/about

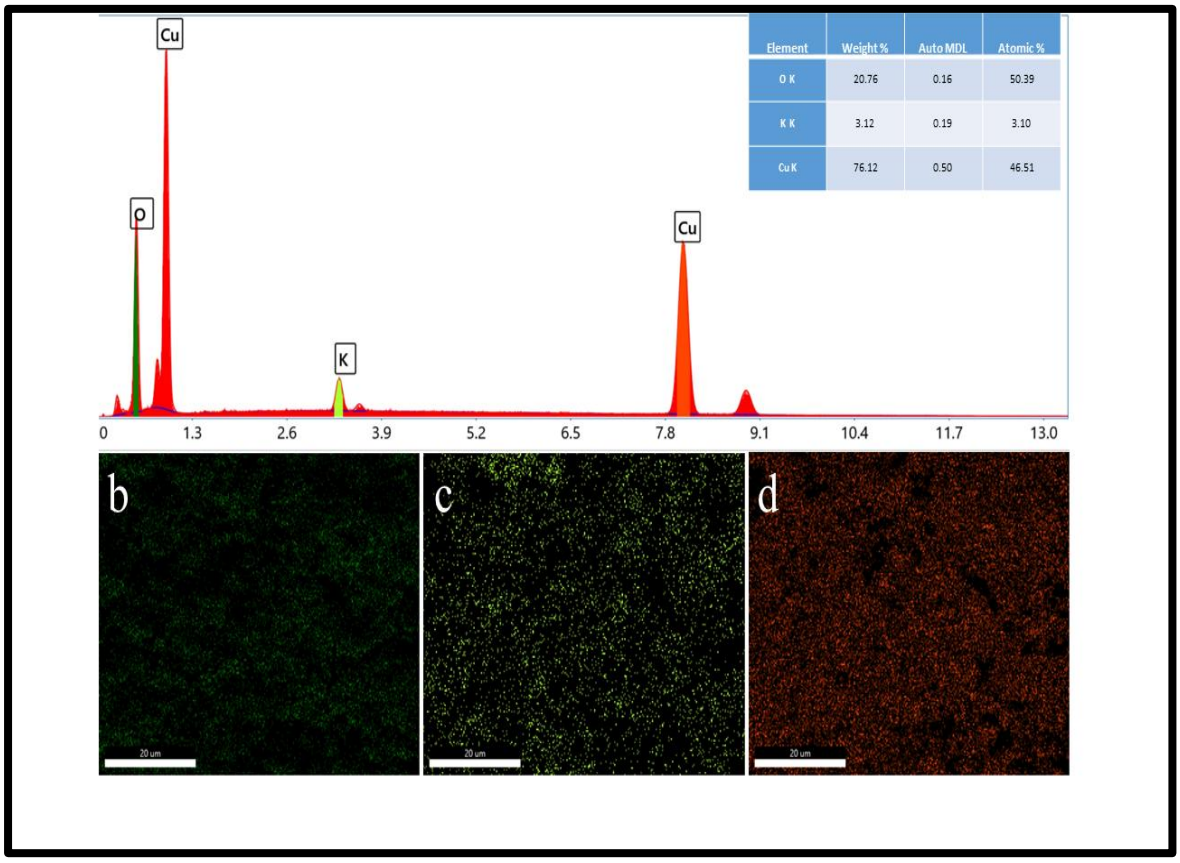


Figure Error! No text of specified style in document..**8:** EDAX analysis with elemental composition and elemental mapping of (i) O (ii) K and (iii) Cu respectively. The elemental mapping of the components found in the Cu, CuO and Cu_2O nanoparticle sample that was synthesized is shown in **Figures 4.8**. Energy dispersion X-ray spectra reveal that the nearly spherical Cu_2O nanostructure particles in

Figure 4.8 contain Cu, O and K with weights of 78.92, 19.06 and 2.03, respectively. According to the appropriate elemental mapping in **Figure 4.8** (i), (ii), and (iii) for Cu nanostructures Cu, O and K are organized well and in relatively tiny amounts, respectively. The absence of additional elements from the EDAX spectrum shows that the generated Cu, CuO and Cu_2O NPs are compatible with the XRD findings [37].

Annual Methodological Archive Research Review
http://amresearchreview.com/index.php/Journal/about
Volume 3, Issue 10 (2025)

Online ISSN 3007-3197
Print ISSN 3007-3189

http://amresearchreview.com/index.php/Journal/about

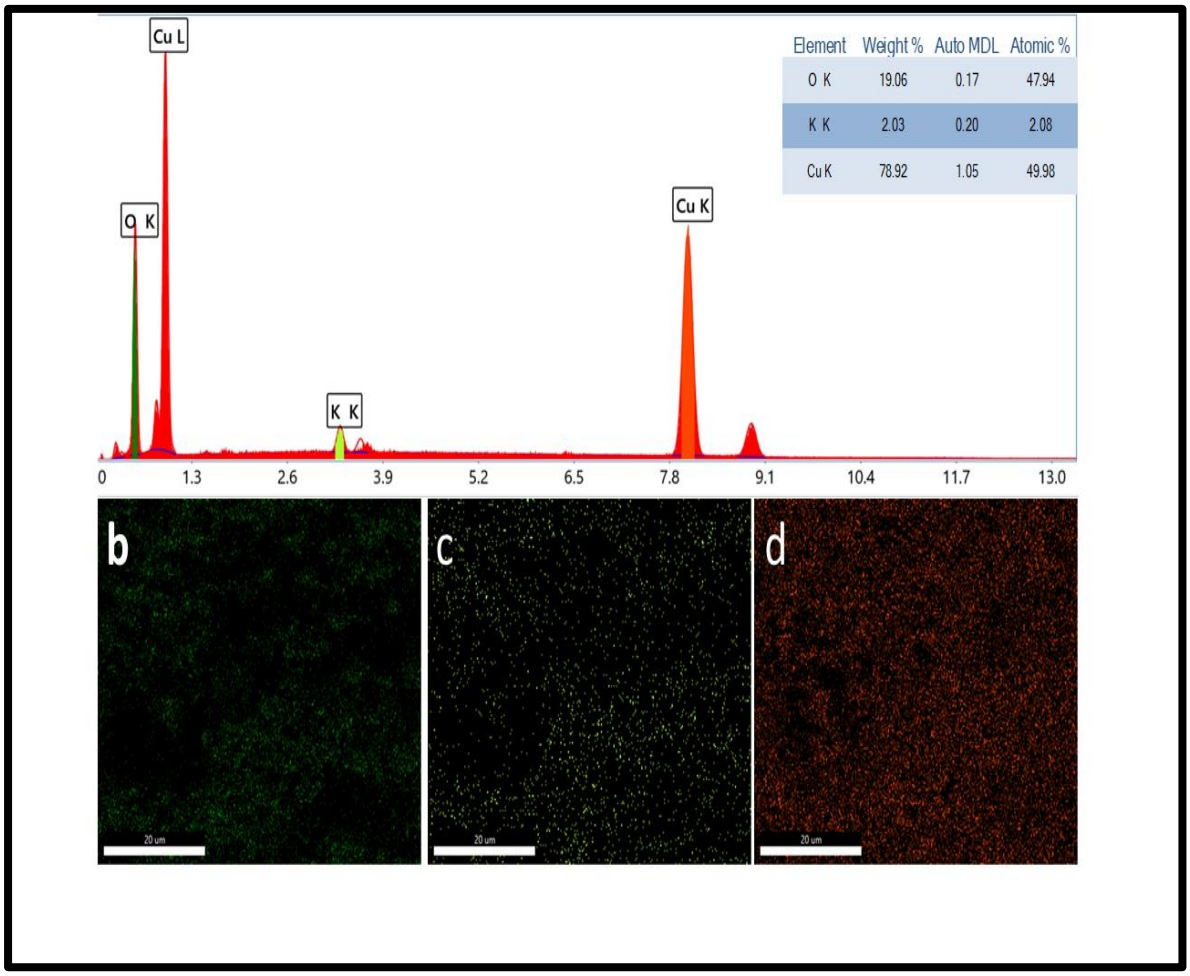


Figure Error! No text of specified style in document..**9:** EDAX analysis with elemental composition and elemental mapping of (i) O (ii) K and (iii) Cu respectively.

Optical Transmittance Spectrum of Copper, Cupric Oxide and Cuprous Oxide Nanoparticles PET Films

The optical transmittance of transparent flexible films and electrodes over a broad wavelength range is a crucial characteristic. To check the optical properties of the hybrid films while they were being formed, the optical transparency of the Cu_2O NPs films was measured with a spectrophotometer. **Figure 4.7** displays the hybrids acquired optical transmittance as a function of various ink transfer rates to the PET films. Optical transmittance that was achieved ranged from a high of 82.37% to a low of 53.23%. In the broad range from 400 nm to 1200 nm, the transmittance values for each of the produced films. The maximum transmittance of the 0.04 ml ink-based PET film was 82.37% [38].

Once the transmitted ink volume exceeded 0.2 mL, the transmittance was significantly reduced. For 0.08 mL to 0.12 mL of ink-based film, a transmittance of 73.82% to 73.85% was attained, there is no change in transmittance. For 0.16 mL, a transmittance of 72.65% was attained. By increasing the concentration up to 0.2 mL

Annual Methodological Archive Research Review
http://amresearchreview.com/index.php/Journal/about
Volume 3, Issue 10 (2025)

Online ISSN 3007-3197
Print ISSN 3007-3189

http://amresearchreview.com/index.php/Journal/about

of ink-based PET films, the transmittance value fell even more to 53.23% [39, 40]. The increased density and conductive networks of Cu_2O NPs, which cause a drop in the sheet resistance and a subsequent decrease in the transmittance of the films may be to blame for the quick loss of transparency. The presence of Cu_2O NPs layers in the ink caused a decrease in the transparency of the composite films. Due to the high density of ink transfer, the substantial transparency reduction also indicates that there is a higher number of Cu_2O NPs present in the composite films, which causes a strong photon absorption in the visible range [41].

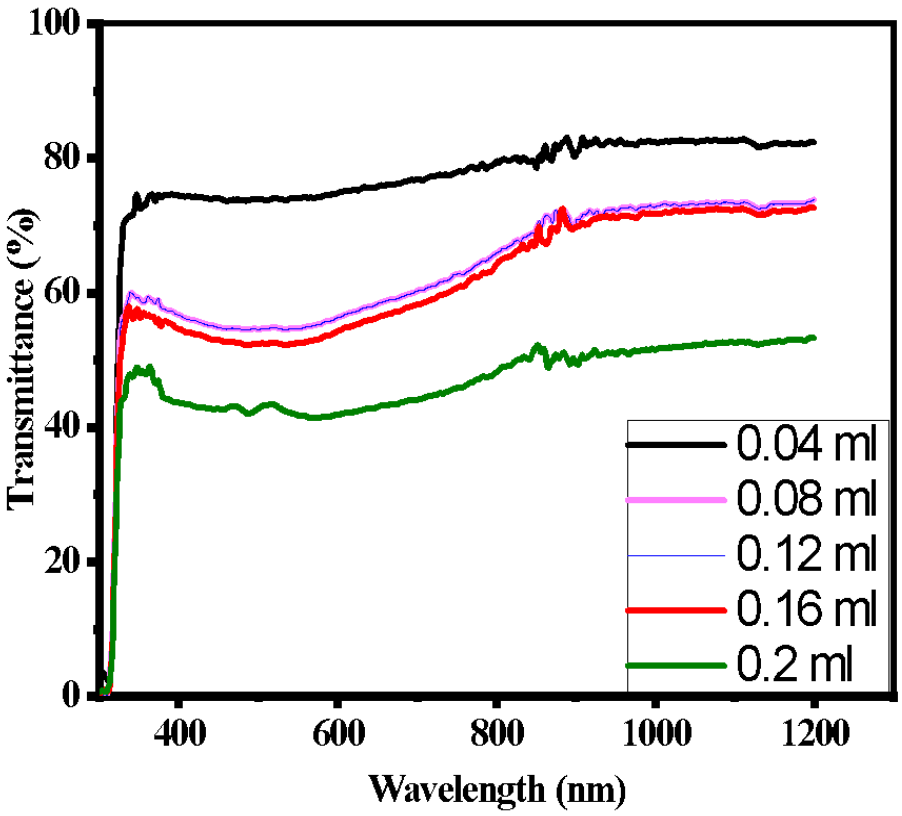


Figure Error! No text of specified style in document.**.10:** The five Cu_2O NPs PET films optical performance with various ratios of ink.

Conclusion

In this work, glucose was used as the reducing agent and $CuCl_2$ as the precursor to create Cu, CuO and Cu_2O NPs by a chemical reduction method. By using X-ray diffraction (XRD), energy dispersive X-ray (EDX) and scanning electron microscopy (SEM), the Cu, CuO and Cu_2O NPs structure and morphology were studied. The generation of Cu, CuO and Cu_2O NPs was confirmed by the UV-Visible absorption spectra, which exhibit peaks at 559, 558 and 557 nm, respectively. The three samples were prepared at different growth temperatures i.e. 60^0, 70^0 and 80^0, named as Cu-T_1, Cu-T_2 and Cu-T_3, respectively. Using Tauc plots and absorption data, the band gaps

Annual Methodological Archive Research Review
http://amresearchreview.com/index.php/Journal/about
Volume 3, Issue 10 (2025)

Online ISSN 3007-3197
Print ISSN 3007-3189
http://amresearchreview.com/index.php/Journal/about

of the Cu-T_1, Cu-T_2 and Cu-T_3 NPs were found to be 2.04 eV, 2.15 eV and 2.21 eV, respectively. The XRD patterns demonstrates the crystalline and monoclinic nature of the Cu, CuO and Cu_2O NPs. The crystallinity of Cu, CuO and Cu_2O NPs was likewise shown to rise with an increase in annealing temperature and the diffraction peaks were made sharper. The intensity of every diffraction peak increases along with the increase in peak concentration. As temperature rises, the intensity of all diffraction peaks rises, but their full width at half maximum (FWHM) falls. It was well known that the width of the diffraction peak increases with crystallinity size. The structural analyses exhibit base-centered spherical nanocrystals with crystallite sizes of 12 nm, 23 nm and 18 nm for the said samples. The SEM images reveal the corresponding non-agglomerated particle diameters of about 310 nm, 200 nm and 100 nm, respectively. EDX analysis validated the elemental quantification and stoichiometry ratio of Cu, CuO and Cu_2O NPs. To obtain the optical responses from Cu_2O NPs, hydroxyl ethyl cellulose (HEC) as an adhesive agent mixed with the sample "Cu-T_3 NPs" was used as an ink and spread on a flexible substrate (Polyethylene-terephthalate/PET) with different dispersion volumes (0 mL, 0.04 mL, 0.08 mL, 0.12 mL, 0.16 mL and 0.2 mL). As prepared flexible substrate-based sample were tested for their transmittance measurements. The maximum transmittance obtained was 82.37% for 0.04 mL dispersion and the minimum value was 53.23% for 0.2 mL dispersion ink, suggesting the Cu_2O NPs desirable candidates for low cost flexible and transparent windows applicable in solar panels and other technologies.

Reference

Alghamdi, H.A., Structural, morphological, optical, and electrical characteristics of polyethylene oxide/chitosan-copper oxide nanoparticles for optoelectronic applications. Optical Materials, 2022. **134**: p. 113101.

Saleem, S., et al., Enhancement in structural, morphological, and optical properties of copper oxide for optoelectronic device applications. Nanotechnology Reviews, 2022. **11**(1): p. 2827-2838.

Dhineshbabu, N.R., et al., Study of structural and optical properties of cupric oxide nanoparticles. Applied Nanoscience, 2016. **6**(6): p. 933-939.

Al-Fa'ouri, A.M., et al., Investigation of optical and structural properties of copper oxide nanoparticles synthesized via green method using Bougainvillea leaves extract. Nano-Structures & Nano-Objects, 2023. **36**: p. 101051.

Nam, V.B. and D. Lee, Copper nanowires and their applications for flexible, transparent conducting films: a review. Nanomaterials, 2016. **6**(3): p. 47.

Nam, V.B., T.T. Giang, and D. Lee, Laser digital patterning of finely-structured flexible copper electrodes using copper oxide nanoparticle ink produced by a scalable synthesis method. Applied Surface Science, 2021. **570**: p. 151179.

Eyovge, C., et al., Color tuning of electrochromic TiO2 nanofibrous layers loaded with metal and metal oxide nanoparticles for smart colored windows. ACS Applied Nano Materials, 2021. **4**(8): p. 8600-8610.

Nguyen, V.H., et al., Advances in flexible metallic transparent electrodes. Small, 2022. **18**(19): p. 2106006.

Kim, H.-S., et al., Optical and electrical properties of Cu-based all oxide semi-transparent photodetector. Applied Physics Letters, 2016. **109**(10).

Online ISSN 3007-3197
Print ISSN 3007-3189

Chavali, M.S. and M.P. Nikolova, Metal oxide nanoparticles and their applications in nanotechnology. SN applied sciences, 2019. **1**(6): p. 607.

Anmar, H.S., Electrical and optical properties of copper oxides thin films on plastic substrates fabricated by helicon plasma sputtering. Kogakuin University.

Saravanakumar, K., et al., Physical and bioactivities of biopolymeric films incorporated with cellulose, sodium alginate and copper oxide nanoparticles for food packaging application. International Journal of Biological Macromolecules, 2020. **153**: p. 207-214.

Atchaya, S. and J. Meena Devi, Experimental Investigation on Structural, Optical, Electrical and Magnetic Properties of Copper Oxide Nanoparticles. Proceedings of the National Academy of Sciences, India Section A: Physical Sciences, 2024. **94**(1): p. 153-160.

Rani, P., et al. Study of structural and optical properties of Fe doped CuO nanoparticles. in AIP Conference Proceedings. 2016. AIP Publishing LLC.

Patwary, M.A.M., et al., Copper oxide nanostructured thin films processed by SILAR for optoelectronic applications. RSC advances, 2022. **12**(51): p. 32853-32884.

Aldossary, A.S. and N. Sulaiman, PCM examine of Silica/Decane nanostructure in the presence of copper oxide nanoparticles to improve the solar energy capacity of glass in the solar collectors via MD approach. Engineering Analysis with Boundary Elements, 2022. **145**: p. 72-82.

Chinky and P. Kumar, Conventional layer free homeotropic alignment and enhanced electro-optic properties of liquid crystals using metal and metal oxide nanoparticles. Journal of Materials Science, 2025: p. 1-30.

Ramos, M.K. and A.J. Zarbin, Graphene/copper oxide nanoparticles thin films as precursor for graphene/copper hexacyanoferrate nanocomposites. Applied Surface Science, 2020. **515**: p. 146000.

Ramos, M.K., et al., Nanoarchitected graphene/copper oxide nanoparticles/MoS 2 ternary thin films as highly efficient electrodes for aqueous sodium-ion batteries. Materials Horizons, 2023. **10**(12): p. 5521-5537.

Tao, P., et al., Preparation and optical properties of indium tin oxide/epoxy nanocomposites with polyglycidyl methacrylate grafted nanoparticles. ACS applied materials & interfaces, 2011. **3**(9): p. 3638-3645.

Kumar, S.S., et al., Synthesis, characterization and optical properties of zinc oxide nanoparticles. International Nano Letters, 2013. **3**(1): p. 30.

Huang, X.-J., et al., Transparent dispersions of monodispersed ZnO nanoparticles with ultrahigh content and stability for polymer nanocomposite film with excellent optical properties. Industrial & Engineering Chemistry Research, 2018. **57**(12): p. 4253-4260.

Kim, H., et al., Fabrication of a semi-transparent flexible humidity sensor using kinetically sprayed cupric oxide film. Sensors and Actuators B: Chemical, 2018. **274**: p. 331-337.

Al-Gunaid, M.Q., A.M. Saeed, and Siddaramaiah, Effects of the electrolyte content on the electrical permittivity, thermal stability, and optical dispersion of poly (vinyl alcohol)–cesium copper oxide–lithium perchlorate nanocomposite solid-polymer electrolytes. Journal of Applied Polymer Science, 2018. **135**(8): p. 45852.

Online ISSN 3007-3197
Print ISSN 3007-3189

Jastaneyah, Z., et al., A comparative analysis of standard and nano-structured glass for enhancing heat transfer and reducing energy consumption using metal and oxide nanoparticles: a review. Sustainability, 2023. **15**(12): p. 9221.

Taghavi Fardood, S., et al., Green synthesis, characterization, photocatalytic and antibacterial activities of copper oxide nanoparticles of copper oxide nanoparticles. Nanochemistry Research, 2023. **8**(2): p. 134-140.

Saleem, M.H., et al., Synthesis, characterization, and advanced sustainable applications of copper oxide nanoparticles: a review. Clean Technologies and Environmental Policy, 2024: p. 1-26.

Mahawar, L., et al., Effect of copper oxide and zinc oxide nanoparticles on photosynthesis and physiology of Raphanus sativus L. under salinity stress. Plant Physiology and Biochemistry, 2024. **206**: p. 108281.

Mavil-Guerrero, E., R. Vazquez-Duhalt, and K. Juarez-Moreno, Exploring the cytotoxicity mechanisms of copper ions and copper oxide nanoparticles in cells from the excretory system. Chemosphere, 2024. **347**: p. 140713.

Liu, H., et al., Size-controlled synthesis of copper oxide nanoparticles with a supercritical hydrothermal synthesis method. Powder Technology, 2024. **444**: p. 119803.

Mathanmohun, M., et al., Unveiling sustainable, greener synthesis strategies and multifaceted applications of copper oxide nanoparticles. Journal of Molecular Structure, 2024. **1305**: p. 137788.

Alshamari, A., A.M. El Sayed, and S. Taha, Developing thermally stable CuO/DPC/PVC nanocomposite films for flexible UV shielding and dielectric applications. Journal of Molecular Structure, 2025. **1343**: p. 142893.

Badawi, A., et al., Exploring the structural and optical properties of Cu1− xNixO/ZnO nanostructured heterojunctions for optoelectronic studies. Applied Physics A, 2024. **130**(5): p. 327.

Pal, S. and D. Basak, Ultrathin Oxide/Metal/Oxide Trilayer Transparent Conducting Electrodes for an All-Transparent Flexible UV Photodetecting Device. ACS Applied Electronic Materials, 2024. **6**(9): p. 7035-7045.

Al-Muntaser, A., et al., Investigation of structural and optical characteristics of PVA/crystal violet dye composites for flexible smart optoelectronic applications. Journal of Polymer Research, 2024. **31**(10): p. 311.

Amin, N., et al., Annealing-induced transformation of structural and optical parameters of transparent γ-CuI thin films with superior thermoelectric performance. Ceramics International, 2024. **50**(19): p. 36884-36891.

Alruwaili, A., et al., Engineered nanoparticle doping, structural, and optical innovations in polyvinyl alcohol composites for advanced optoelectronic applications. Journal of Thermoplastic Composite Materials, 2025: p. 08927057251344132.

Madshal, M., M. Mundher, and N. Albogamy, Structure and optical properties of copper sulfate-filled carboxymethyl cellulose/sodium alginate polymer composite thin films. Journal of Materials Science: Materials in Electronics, 2025. **36**(16): p. 1-13.

Boscarino, S., et al., Cu metal nanoparticles in transparent electrodes for light harvesting in solar cells. Applied Surface Science, 2024. **655**: p. 159547.

Online ISSN 3007-3197
Print ISSN 3007-3189

Wang, X., et al., Polymer stabilized cholesteric liquid crystals enhanced by functional nanofibers loaded with CuS NPs and ATO NPs for efficient smart windows and advanced infrared camouflage/anti-counterfeiting technologies. Applied Materials Today, 2025. **42**: p. 102540.

Nouh, S., et al., Tailoring the optical and color properties of gamma-irradiated PC/CuO nanocomposite films for their application in optoelectronic devices. Radiation Effects and Defects in Solids, 2025. **180**(1-2): p. 209-226.